

Rapid structural and chemical characterization of ternary phase diagrams using synchrotron radiation

E.D. Specht^{a)}

Metals and Ceramics Division, Oak Ridge National Laboratory, Oak Ridge, Tennessee 37831

A. Rar, G.M. Pharr, and E.P. George

Metals and Ceramics Division, Oak Ridge National Laboratory, Oak Ridge, Tennessee 37831 and Department of Materials Science and Engineering, University of Tennessee, Knoxville, Tennessee 37996

P. Zschack and H. Hong

Frederick Seitz Materials Research Laboratory, University of Illinois at Urbana-Champaign, Urbana, Illinois 61801

J. Ilavsky

National Institute of Standards and Technology, Gaithersburg, Maryland 20899

(Received 19 May 2003; accepted 31 July 2003)

A technique based on synchrotron radiation was developed that allows for rapid structural and chemical characterization of ternary alloys over a wide range of composition. The technique was applied to isothermal sections of the Cr–Fe–Ni system grown on Al₂O₃(0001) sapphire substrates by sequential deposition of layers of graded thickness followed by annealing to interdiffuse the elements. A film spanning the Cr–Fe–Ni ternary system was measured in 4 h at a resolution of 2 at.% by rastering the sample under a focused beam of synchrotron radiation while simultaneously measuring the diffraction pattern with a charge-coupled device detector to determine crystallographic phases, texture, and lattice parameters and also measuring the x-ray fluorescence with an energy-dispersive detector to determine elemental composition. Maps of phase composition and lattice parameter as a function of composition for several annealing treatments were found to be consistent with equilibrium values. The technique will be useful in combinatorial materials design.

I. INTRODUCTION

Development of new materials by combinatorial synthesis and design has recently received much attention due to the potential it offers for discovering new materials and improving existing ones.^{1–3} Combinatorial materials science is based on two key elements: (i) simple synthesis techniques that can be used to create large libraries of specimens of varying composition and structure, and (ii) simple characterization techniques that can be used to rapidly assess the structure and properties of the material libraries.

One popular method for synthesizing combinatorial material libraries uses vapor deposition or sputtering to make thin films in which the composition varies continuously in the plane of the film. The composition gradient is created by controlling the geometry and position of the component sources and/or the use of shutters and masks.¹ Some techniques require that the specimen be annealed after deposition to intermix and react the components by

solid-state diffusion. By these methods, high-quality films with compositions varying continuously across the binary or ternary phase system have been produced.^{4–7}

Point-to-point characterization of the crystal structures and compositions of the phases in the thin-film material libraries can be used to determine the binary or ternary equilibrium phase diagrams, a technique deemed continuous phase diagram (CPD) determination.⁴ X-ray fluorescence (XRF), x-ray diffraction (XRD), and electron microprobe analysis are all useful CPD tools,^{4–8} but to be applied efficiently to a large number of material compositions, the techniques must provide for rapid data collection and analysis.⁹ Here, we describe a technique based on XRD and fluorescence using synchrotron radiation to achieve these goals. The technique is applied to the Fe–Ni–Cr ternary metallic alloy system, which constitutes a large number of technologically important metallic materials such as stainless steel, invar, and nichrome. The technique was used to fully characterize the structure and composition of ternary alloy films annealed at approximately 850 °C, from which isothermal sections of the phase diagram and contour maps of lattice parameters were constructed. Approximately 2500 compositions were examined in a single experiment taking

^{a)}Address all correspondence to this author.
e-mail: specht@ornl.gov

about 4 h. The rapid rate of characterization is possible due to the short data acquisition time [1 s to expose the charge coupled device (CCD), 5 s to read the CCD, 1 s to move the specimen] and the computer-controlled automation of the process using a precision specimen-positioning table. Results obtained by the method are compared to the well-established phase diagram and lattice parameter measurements.

II. EXPERIMENTAL

The samples were prepared by physical vapor deposition followed by annealing. In brief, sequential layers of Fe, Ni, and Cr were deposited on Al₂O₃(0001) sapphire substrates, 50 mm in diameter, by electron beam evaporation system in a vacuum of 10⁻⁶ to 10⁻⁷ torr. The average deposition rate was about 1 nm/s, as measured with a quartz microbalance. Each layer was grown with a linear thickness gradient by sliding a stepping motor driven shutter located between the specimen and the evaporation target. After a layer was deposited, the sample was rotated 120° for deposition of the next layer. This resulted in a triangular region with an elemental distribution close to that of the composition triangle of a standard ternary phase diagram. The order of the layers and the maximum thickness of each layer are listed in Table I.

The layers were alloyed by annealing at approximately 850 °C in a vacuum of 5 × 10⁻⁷ torr. The heating time and heating conditions required to interdiffuse the layers were estimated in previous work^{10,11} and confirmed by angular-resolved XRF and cross-sectional scanning electron microscopy with energy-dispersive x-ray spectroscopy. The details on the sample preparation procedures and resulting layer structures will be published elsewhere.¹²

XRD and fluorescence data were collected at beamline 33-ID-D of the Advanced Photon Source, Argonne, IL. Undulator radiation, monochromatized to 15 keV by Si(111) crystals and focused to approximately 0.25 × 0.5 mm², was incident on the sample at a 15° glancing angle, giving a 1.0 × 0.5 mm² footprint on the sample. The incident beam was filtered with a 0.25-mm Ti foil (1.7% transmission) to avoid saturating the detectors

(future experiments can use a less intense x-ray source). The sample was mounted on a five-axis translation/rotation system: from bottom to top, we have a raster motion transverse to the incident beam, a rotation to set the glancing angle, a raster motion in the plane of the sample along the beam, and two tilts to align the sample plane with the plane spanned by the raster motions.

Incident beam intensity was monitored with an air-filled ion chamber. Diffraction patterns were recorded by a 1024 × 1024 x-ray CCD camera with 60-μm pitch, located 10 cm behind the sample. Fluorescence was measured by a thermoelectrically cooled, Si positive-intrinsic-negative (PIN) photodiode, with the Cr, Fe, and Ni K_α intensities each recorded using a single-channel analyzer. The sample was rastered on a 1 × 1 mm² grid, with a set of data collected at each point at 7-s intervals. Data was collected for the circular substrate in 4 h, of which 2 h was spent scanning the triangular ternary system; that is, data collection time could be halved by carefully defining the area to be scanned.

The fluorescent intensities at each point on the samples were used to find the elemental compositions. Because of the limited energy resolution of the photodiode, there was some crosstalk: Cr K_β radiation produced signal on the Fe K_α channel and Fe K_β on Ni K_α. Crosstalk was measured using the pure metal corners of the specimen and was corrected for by subtracting an appropriate fraction of the Cr and Fe signals from those of Fe and Ni, respectively. The corrected fluorescence F_A from element A was related to the densities c_B of each element B by

$$F_A = d_A I \int_0^T \exp\left(-\frac{z \sum_B \sigma_B c_B}{\sin \theta} - \frac{z \sum_B \sigma'_B c_B}{\sin \theta'}\right) dz,$$

where I is the incident beam intensity, T is the film thickness, σ_B and σ'_B are the absorption cross sections for incident and fluorescent x rays by element B ,¹³ and $\theta = 15^\circ$ and $\theta' = 56^\circ$ are the glancing angles for incident and fluorescent x rays. The constants d_A for each element, which depend on the fluorescence cross section, absorption by air, and the efficiency of the detectors for incident and fluorescent x rays, were found by measuring fluorescence from the pure elements. Ratios of the fluorescence intensities at each point can be measured more accurately than the absolute intensities because the ratios are not affected by dead time in the detectors or by dark current in the incident-beam monitor, so at each point least-squares refinement was used to find the ratios $c_A/\sum_B c_B$ which give a best fit to the measured ratios $F_A/\sum_B F_B$, subject to the constraint that $\sum_B c_B = c_i$; we approximate $c_i = 8.65 \times 10^{22}/\text{cm}^3$.

Diffraction patterns were analyzed using the FIT2D package.^{14,15} A diffraction pattern from a standard polycrystalline Al₂O₃ sample (NIST SRM 1976) was used to

TABLE I. Sample specifications.

Sample	Layers	Annealing
A	Ni(1.85 μm)/Fe(1.6 μm)/ Cr(1.7 μm)/Al ₂ O ₃ (0001)	20 h, 850 °C, vacuum
B	Ni(2 μm)/Fe(2.5 μm)/ Cr(2.5 μm)/Al ₂ O ₃ (0001)	2 h, 825 °C, vacuum
C	Ni(0.74 μm)/Fe(1.7 μm)/ Cr(1.56 μm)/Ni(0.827 μm)/ Al ₂ O ₃ (0001)	20 h, 850 °C, vacuum

find the sample–CCD distance and direct beam location on the CCD. The two-dimensional images were then integrated without further correction to yield one-dimensional scans of intensity versus plane spacing.¹⁴ Composite two-dimensional images were constructed in which each row corresponds to one integrated diffraction pattern; phase boundaries were visible on these composite images. Quantitative analysis of lattice parameters and peak intensities were performed by least-squares fitting to one-dimensional scans.¹⁶

Lattice parameters were sensitive to sample displacements: a displacement of 0.1 mm is calculated to cause an error of approximately 0.2% in lattice parameter. A linear correction was made to lattice parameters to match the bulk value for pure elements at the corners of the phase diagram to correct for sample displacement and tilt. This calibration procedure also removed the effects of residual stress (caused by differential thermal expansion between the substrate and film), assuming that the strain is uniform across the ternary section.

III. RESULTS AND DISCUSSION

The measured elemental composition of sample A is shown in Fig. 1. Lines are contours of 0, 10, . . . 90 at.% Cr, Fe, and Ni. Small deviations from the intended linear composition profiles are visible and are corrected for in the ternary diagrams that follow. Similar corrections are made for the other samples.

A typical CCD image is shown in Fig. 2, including an epitaxial bcc phase and a weakly textured face-centered cubic (fcc) phase. Because the body-centered cubic (bcc) phase is so much better aligned, it scatters much more strongly at its peak, and a conventional $\theta/2\theta$ scan incorrectly indicates that the fcc is a trace phase relative

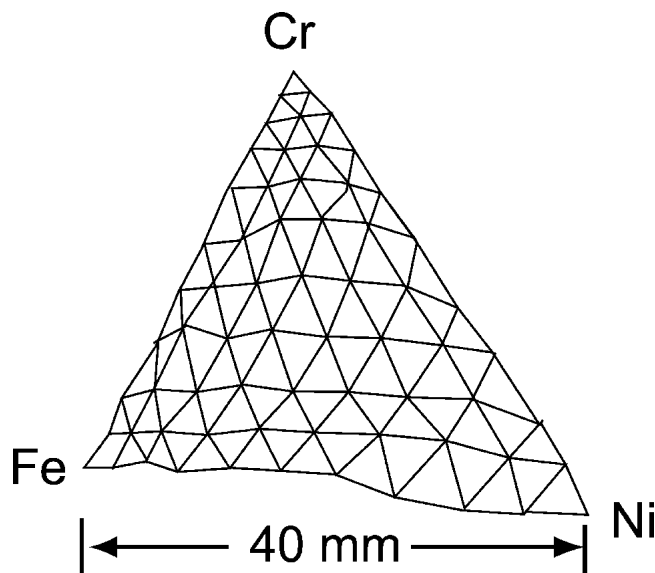


FIG. 1. Geometrical locations of the ternary composition grid on sample A. Lines are contours of 0, 10 . . . 90 at.% Cr, Fe, and Ni.

to the bcc, as would a scan taken with a linear detector. Integrating the CCD image correctly shows that both are major components.

Integrated powder patterns for the various phases are shown in Fig. 3. We observe the three equilibrium phases in the Cr–Fe–Ni system. The bcc or α phase is the structure of Fe and Cr, and the fcc or γ phase is that of Ni. A tetragonal intermetallic σ phase occurs as the metals approach the $\text{Cr}_{50}\text{Fe}_{50}$ composition. Cr_2O_3 can be seen in the Cr-rich compositions due to residual oxygen during annealing.

Relative peak intensities show the crystallographic texture. For a randomly oriented film, relative peak intensities will be the same as for a random powder. Deviations are due to preferred orientation; pole figures using a conventional x-ray system show that the highly textured phases we observe are in fact fully epitaxial. The bcc phase is weakly textured except for compositions near pure Fe, where it is epitaxial with $\text{bcc}(110)\parallel\text{Al}_2\text{O}_3(0001)$ and $\text{bcc}\langle 110\rangle\parallel\text{Al}_2\text{O}_3\langle 11\bar{2}0\rangle$ or $\langle 10\bar{1}0\rangle$. The face-centered-cubic (fcc) phase is weakly textured at high Cr concentrations, while at low Cr concentrations it is epitaxial with $\text{fcc}(110)\parallel\text{Al}_2\text{O}_3(0001)$ with poorer alignment than the epitaxial body-centered-cubic (bcc) phase. The σ phase is randomly oriented.

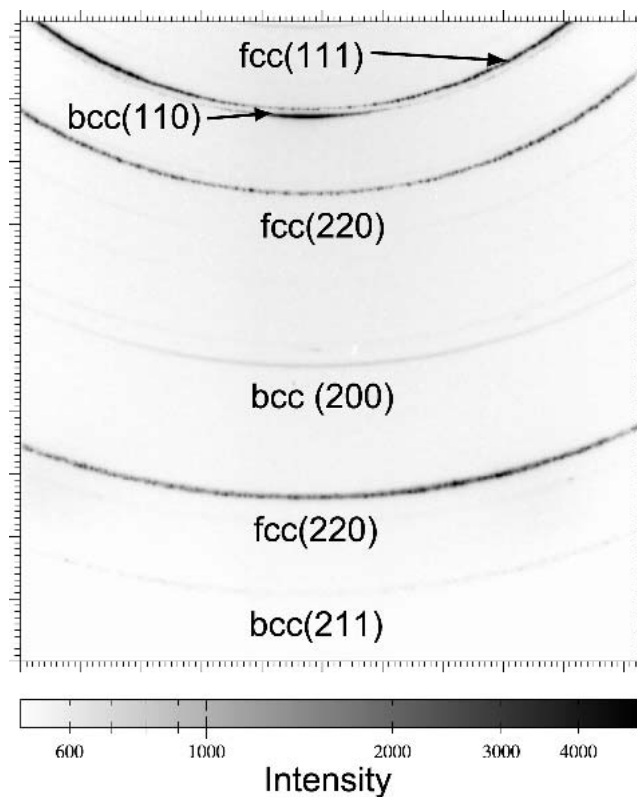


FIG. 2. CCD image from $\text{Fe}_{10}\text{Cr}_{60}\text{Ni}_{30}$ on sample A, illustrating a weakly textured fcc phase and a bcc phase with (110) epitaxy. Weak, unlabeled peaks are from Cr_2O_3 . Note the log scale: the $\text{bcc}(110)$ scattering is 50 times as intense as the $\text{bcc}(200)$.

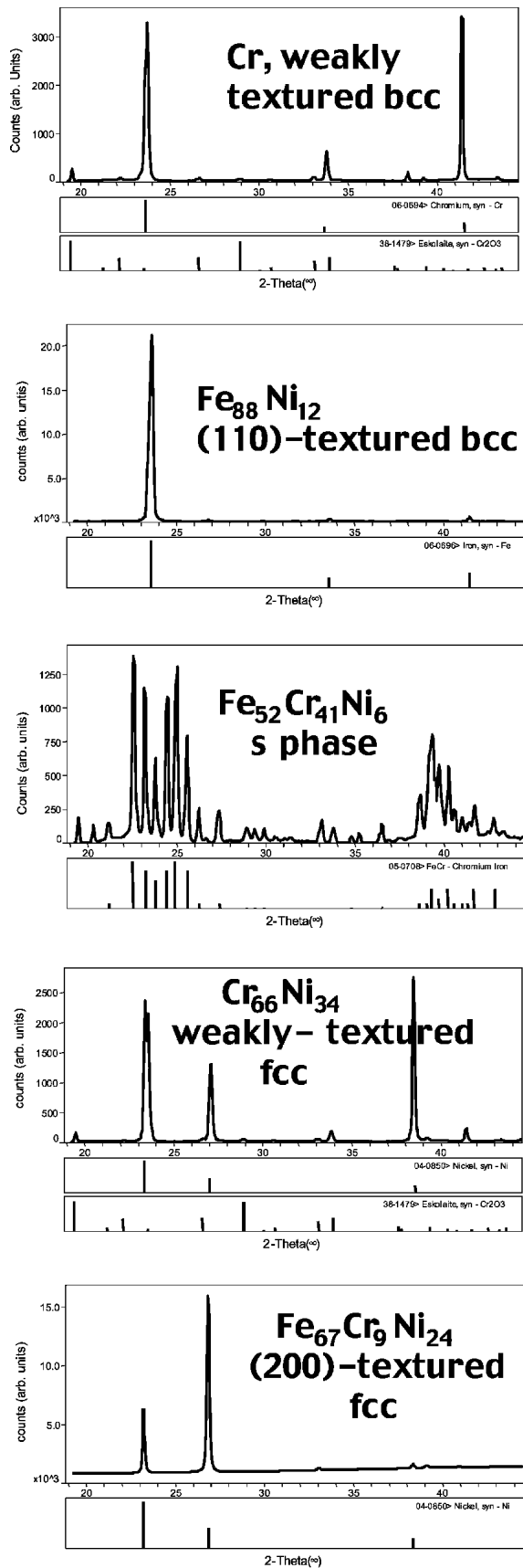


FIG. 3. Integrated powder patterns for phases occurring in A.

A composite image of 49 scans, forming one row along the sample, is shown in Fig. 4, illustrating the appearance of the various phases. The identification of phase boundaries has not successfully been automated, in part due to the complication of epitaxy: various diffraction lines may be either missing or very intense, depending on the alignment of the film. We have recently observed that growth on the (11 $\bar{2}$) surface of Al₂O₃ produces films with much more random alignment. Use of this surface may permit automation of this tedious step.

Ternary phase diagram sections for the three samples are shown in Fig. 5, along with the known equilibrium phase diagram section for 850 °C.¹⁷ The agreement is generally good. The least-annealed sample, B, has a larger three-phase region than the calculated section and no single-phase σ region. This is to be expected for an under-annealed sample because the samples are all grown as laminates of bcc and fcc phases and become single phase only by interdiffusion. The more-annealed samples, A and C, show fcc single-phase regions extending much further into the Cr-rich area than expected. This is to be expected from the unintended oxidation of these samples. Cr₂O₃ is observed to form on the Cr-rich material, leaving the metal deficient in Cr. The phase boundary will therefore be at a composition with less Cr than

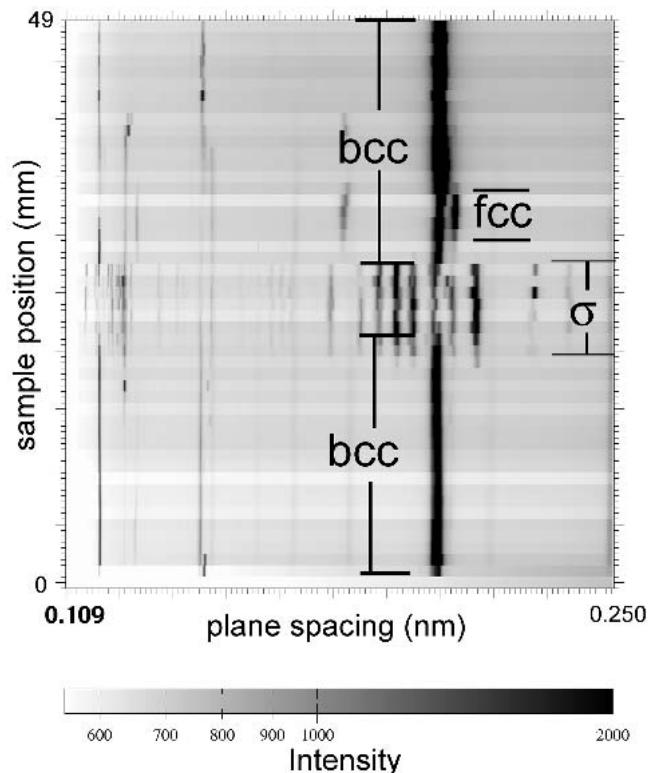


FIG. 4. Composite image. Each row of the composite corresponds to an integrated CCD image from A as it is translated under the x-ray beam in one line of the raster pattern covering the entire sample. The ranges over which each phase is observed are indicated. Weak, unlabeled lines are due to Cr₂O₃.

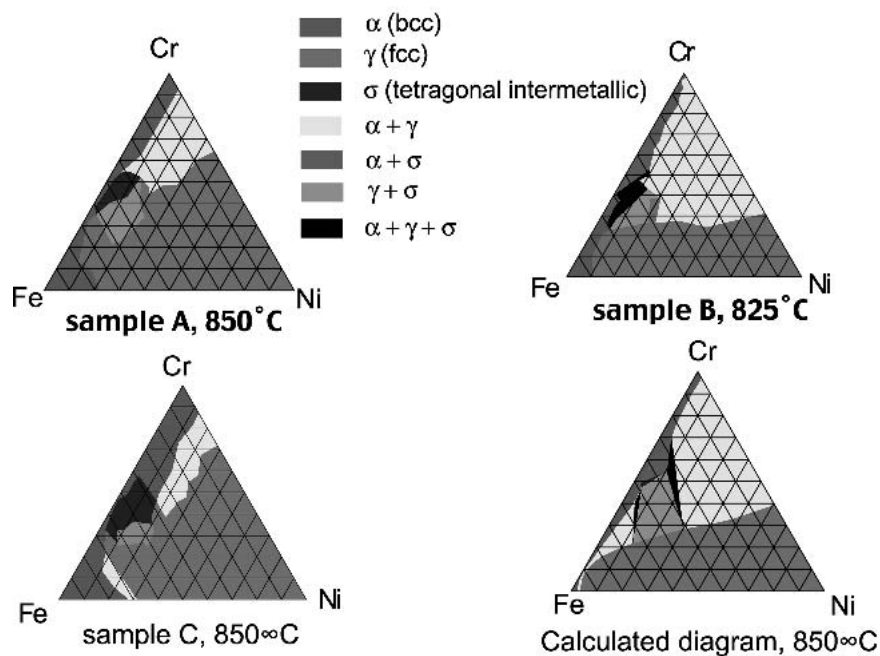


FIG. 5. Measured phase diagram sections compared to that calculated by Chuang *et al.*¹⁷

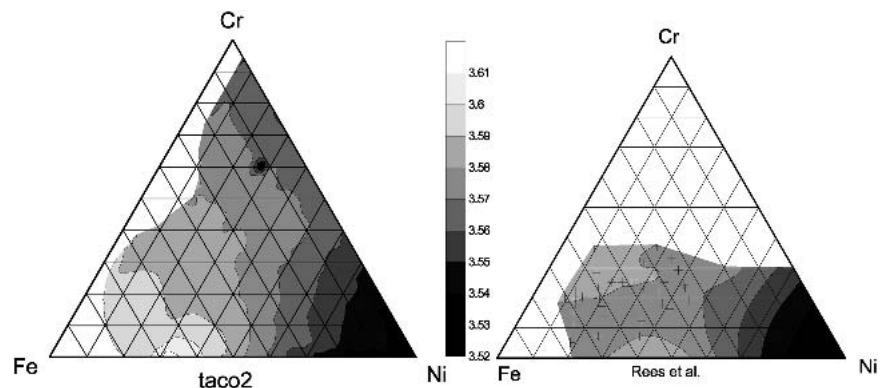


FIG. 6. Lattice parameter from fcc (200) reflection from A compared to results of Rees *et al.*¹⁸

indicated by the fluorescence measurement. A and C were deposited with different layer sequences, but still yield similar phase diagram sections, which suggests that these are indeed equilibrium results. Abrupt transitions from single-phase α to σ confirm that the measurement achieves resolution of 2 at. %.

There is no significant variation in the lattice parameter of the bcc or σ phases. The lattice parameter for the fcc phase, calculated from the (200) reflection of sample A, is shown in Fig. 6, along with the results obtained by conventional methods.¹⁸ The agreement is generally good, although some artifacts can be seen along the line of zero Cr concentration, presumably due to starting of the shutter motion. As expected, lines of constant lattice parameters follow tie lines across the two-phase fcc–bcc region.

IV. CONCLUSIONS

We find that a focused beam of synchrotron radiation can be used to provide rapid structural analysis of combinatorial libraries. The diffraction pattern identifies both epitaxial and randomly oriented phases and gives lattice parameters while the fluorescence can be used to find the elemental composition. Future work will focus on techniques to bring reliably samples to equilibrium conditions.

ACKNOWLEDGMENTS

Work sponsored by the U.S. Department of Energy (U.S. DOE), Division of Materials Sciences and Office of Industrial Technologies, Industrial Materials for the Future Program, under Grant No. DE-FC07-02ID14251.

Oak Ridge National Laboratory (ORNL) is operated by UT-Battelle, LLC, for the U.S. DOE under Contract No. DE-AC05-00OR22725. The UNICAT facility at the Advanced Photon Source (APS) is supported by the University of Illinois at Urbana-Champaign, Materials Research Laboratory (U.S. DOE, the State of Illinois-IBHE-HECA, and the NSF), the Oak Ridge National Laboratory (U.S. DOE under contract with UT-Battelle LLC), the National Institute of Standards and Technology (United States Department of Commerce), and UOP LLC. The APS is supported by the U.S. DOE, Basic Energy Sciences, Office of Science under Contract No. W-31-109-ENG-38.

REFERENCES

1. X.D. Xiang, *Annu. Rev. Mater. Sci.* **29**, 149 (1999).
2. E.W. McFarland and W.H. Weinberg, *Trends Biotechnol.* **17**, 107 (1999).
3. J.C. Zhao, M.R. Jackson, L.A. Peluso, and L.N. Brewer, *MRS Bull.* **27**(4), 324 (2002).
4. Y.K. Yoo and F. Tsui, *MRS Bull.* **27**(4), 316 (2002).
5. T. Fukumura, M. Ohtani, M. Kawasaki, Y. Okimoto, T. Kageyama, T. Koida, T. Hasegawa, Y. Tokura, and H. Koinuma, *Appl. Phys. Lett.* **77**, 3426 (2000).
6. Y.K. Yoo, F. Duewer, T. Fukumura, H.T. Yang, D. Yi, S. Liu, H.Y. Chang, T. Hasegawa, M. Kawasaki, H. Koinuma, and X. Xiang, *Phys. Rev. B* **63****22**, 224421 (2001).
7. Y.K. Yoo, T. Ohnishi, G. Wang, F. Duewer, X.D. Xiang, Y.S. Chu, D.C. Mancini, Y.Q. Li, and R.C. O'Handley, *Intermetallics* **9**, 541 (2001).
8. J.C. Zhao, *J. Mater. Res.* **16**, 1565 (2001).
9. E.D. Isaacs, M. Marcus, G. Aeppli, X-D. Xiang, X-D. Sun, P. Schultz, H-K. Kao, G.S. Cargill, and R. Haushalter, *Appl. Phys. Lett.* **73**, 1820 (1998).
10. C.E. Campbell, W.J. Boettinger, and U.R. Kattner, *Acta Mater.* **50**, 775 (2002).
11. B. Jönsson, *ISIJ Int.* **35**, 1415 (1995).
12. A. Rar, E.D. Specht, G.M. Pharr, and E.P. George (unpublished).
13. W.H. McMaster, N. Kerr Del Grande, J.H. Mallett, and J.H. Hubbell, *Compilation of X-Ray Cross Sections* Report No. UCRL-50174-SEC 2-R-1, (University of California, Livermore, CA, 1969).
14. A.P. Hammersley, FIT20 V10.3 Reference Manual V4.0, ESRF Internal Report No. ESRF98HA01T (ESRF, Grenoble, France, 1998).
15. A.P. Hammersley, S.O. Svensson, M. Hanfland, A.N. Fitch, and D. Häusermann, *High Press. Res.* **14**, 235 (1996).
16. A.P. Hammersley and C. Riekel, *Synchrotron Radiation News* **2**, 24 (1989).
17. Y-Y. Chuang and Y.Y. Chang, *Metall. Trans. A* **18**, 733 (1987).
18. W.P. Rees, B.D. Burns, and A.J. Cook, *J. Iron Steel Inst.* **162**, 325 (1949).